

Effects of finite spin-orbit splitting on optical properties of spherical semiconductor quantum dots

Tristan Richard, Pierre Lefebvre, Henry Mathieu, and Jacques Allègre

*Groupe d'Etude des Semiconducteurs—Centre National de la Recherche Scientifique, Université Montpellier II-CC, 074-34095
Montpellier Cedex 5, France*

(Received 19 June 1995; revised manuscript received 14 September 1995)

The multiband envelope-function formalism—of which a convenient, analytical formulation is presented—is used to investigate the energies and wave functions of valence-band levels in spherical nanocrystallites of several III-V and II-VI compound semiconductors with finite spin-orbit splitting energy Δ . Interband absorption spectra are deduced. A significant influence of the split-off band is found even in cases where Δ is large, as for CdTe. In fact, Δ is not a decisive criterion for the strength of couplings; Luttinger parameters play a major role. Numerical results are presented for size-distributed crystallites of various binaries (CdTe, CdSe, CdS, GaAs, InP). These are analyzed in terms of the accuracy of measuring the sizes from absorption spectra by using a fitting procedure, and of performing size-selective excitation of photoluminescence. It is also found that optical transitions between the ground valence- and conduction-band levels may be forbidden, due to incompatible symmetries. Calculations neglecting the influence of the split-off band are unable to account for this property, which strongly affects photoluminescence mechanisms.

I. INTRODUCTION

Nanometric semiconductor crystallites have recently attracted considerable interest because they represent the materialization of the simple quantum-mechanical problem of quantum boxes. Moreover, their optical properties, strongly influenced by the three-dimensional confinement of carriers, seem to be promising routes to future all-optical data processing devices. In practice, III-V and II-VI semiconductor nanocrystals embedded in glasses, polymers, or in colloids have been prepared by a variety of techniques. The major part of the available work has been done in CdS,¹⁻⁵ CdSe,⁶⁻¹⁰ and CdS_xSe_{1-x} crystallites. Recently, several attempts have led to the fabrication of CdTe,¹¹⁻¹⁴ GaAs,¹⁵ or InP clusters,¹⁶ among other materials.

From the theoretical viewpoint, several previous studies have demonstrated that, for realistic semiconductor systems, the electronic states cannot really be considered as those of a simple particle-in-a-box problem. As a matter of fact, it is now established that the superimposition of a three-dimensional confinement potential, with spherical symmetry, onto the Hamiltonian of a cubic semiconductor leads to complex mixings of valence-band states. These complicate the assignment of quantized levels and of related optical transitions towards conduction-band states. This way to consider electron and holes separately is naturally restricted to the so-called strong confinement regime, i.e., to crystal radii smaller than ~ 2 exciton Bohr radii.¹⁷ Recent works have been devoted to the theoretical study of the quantization of hole states in spherical semiconductor nanocrystallites. Apart from a particular attempt based on a tight-binding approach,¹⁸ most works on this subject were kept within the framework of a multiband effective-mass approximation.¹⁹⁻²⁵ In some cases,^{21,24} a numerical approach was used to solve the set of coupled differential equations which arise from the boundary condition that the wave function be zero at the surface of the crystallite. Moreover, for the sake of simplicity, many authors have treated spin-orbit split-off

(SO) states in one of the asymptotic approximations: $\Delta \rightarrow \infty$,^{20,21,23-25} or $\Delta \rightarrow 0$,²⁰ where Δ is the spin-orbit splitting energy.

Only few recent works^{19,22,23} have faced the problem in a tractable, analytical way. Basically, all approaches are rather similar, since they start from the same so-called six-band Hamiltonian of cubic semiconductors with finite Δ . Ekimov *et al.*¹⁹ have given the basic equations providing the energies of quantized levels in CuCl and solved them by making some approximations. Grigoryan *et al.*²² have given another rigorous general formulation of the necessary equations. Although analytical, these formalisms are not easy to handle and do not provide a convenient assignment of the mixed states. To this extent, Ramaniah and Nair¹⁸ have remarked that the most adapted formalism is an extension of that developed by Baldereschi and Lipari²⁶ for acceptor states in cubic semiconductors, which was adopted by several workers.^{14,18,21,24} The formalism is based on the fact that the total Hamiltonian of the system commutes with operator $F = L + J$. J is the good quantum number for valence states of the cubic semiconductor: $J = \frac{3}{2}$ for light-hole and heavy-hole bands, while $J = \frac{1}{2}$ for the SO band. L would be the good quantum number for a system with the only spherical symmetry of the crystallite. This permits us to deal with a block-diagonal Hamiltonian, where each block corresponds to a given eigenvalue of F ($\frac{1}{2}, \frac{3}{2}, \frac{5}{2}, \dots$).

Sercel and Vahala²³ have thoroughly developed an analytical formulation for cases where $\Delta \rightarrow \infty$, which we call the two-band (2B) modeling, and only for $F = \frac{1}{2}$ and $\frac{3}{2}$. In what follows, we start by extending this convenient 2B modeling to F up to $\frac{7}{2}$, within the same formalism.¹⁴ The main result of such calculations is that “pure” S , P , D , etc. states, which would result from a simplistic one-band approach, are mixed, leading to new states labeled $nP_{1/2}$, $nD_{1/2}$, $nSD_{3/2}$, $nPF_{3/2}$, $nPF_{5/2}$, etc. In these notations, capital letters indicate which kind of L states are coupled (they always differ by two units), n is the principal quantum number, and the

index corresponds to the value of F . Within the 2B model, conduction-band and SO-band states are labeled nS_e , $nP_e, \dots, nS_{SO}, nP_{SO}, \dots$, after their L value, since they are assumed decoupled from the two upper valence-bands. In addition, simple “selection rules” apply: allowed interband transitions occur only between valence-band and conduction-band levels having common orbital quantum numbers L .

As stated above, many workers have adopted the 2B approximation,^{20,21,23–25} for simplicity. This may be an expression of the common intuition that split-off states should play a minor role in materials with large values of Δ , such as CdSe (420 meV) or CdTe (927 meV), especially if one is only concerned by fundamental hole levels.

It is the purpose of this paper to demonstrate that this intuition is misleading: there can be a strong influence of the spin-orbit split-off band on electronic levels of spherical semiconductor quantum dots, even for some materials with large Δ splittings. This work is organized as follows. In the next section, we introduce a convenient way to account exactly for valence-band mixings in spherical crystallites of cubic semiconductors. By solving a few simple equations, we obtain the energies of hole eigenstates and the oscillator strengths of all allowed interband transitions within a range of ~ 1 – 2 eV above the fundamental gap of the system. This work can be achieved with a simple desktop computer, which is of great interest for experimentalists. In Sec. III, we apply this formalism to the calculation of hole levels and of interband absorption spectra of nanocrystals of several popular III-V and II-VI compound semiconductors. We compare the results of 2B and 3B modelings and draw conclusions on the measurable influence of the SO band. The work is summarized in Sec. IV.

II. MODELING OF CONFINED STATES

Within the framework of the envelope-function formalism, we consider the crystallites as spherical clusters surrounded by an infinitely high potential barrier. Then, the angular and radial parts of the wave functions are separable. The eigenfunctions of the problem are the product of spherical harmonics (quantum numbers L and m), for the angular variation, by radial functions. The condition of vanishing of these radial functions at the surface of the sphere ($r=R$) provides the stationary states of the system. In the treatment of valence bands, we made the so-called spherical approximation, i.e., the following relationship between Luttinger parameters: $\gamma_2 = \gamma_3$.

The simplest approach of confined electronic states consists in a one-band effective-mass approximation, where conduction and valence bands are all assumed parabolic, isotropic, and independent, and where no difference is made between the so-called light-hole and heavy-hole states. In most usual semiconductors of interest (CdS, CdSe, CdTe, GaAs, InP, etc.) the energy gap is large enough to make this approximation quite reasonable for conduction states. This one-band approximation will thus be assumed relevant along the rest of this work, for conduction states.

A. One-band approximation

The conduction-band energy is given, versus the wave number K , by $E = E_c + K^2/2m_e$ (we assume units such that

$\hbar = 1$). Both valence bands are then represented by a common dispersion relation, $E = E_v - \gamma_1 K^2/2$, while the spin-orbit split-off band is given by the equation $E = E_v - \Delta - \gamma_1 K^2/2$. E_c and E_v are the energies at the Γ point, at the bottom of conduction band, and at the top of valence bands, respectively.

In this simplistic approach, the Hamiltonian commutes with the angular momentum operator L^2 . Thus, the wave functions, for all types of carriers, are given by spherical harmonics $Y_L^m(\theta, \varphi)$, multiplied by spherical Bessel functions $j_L(Kr)$, for the radial variation. The boundary condition then takes the form $j_L(KR) = 0$, which is fulfilled by an infinity of discrete values K_n , where n is the principal quantum number. The orbital number L defines the type of the quantized state. Such states will be termed “pure” S -, P -, D -like (etc.) states, in the following, for $L=0, 1, 2, \dots$, respectively. Their degeneracies are equal to $(2L+1)$.

Concerning optical transitions, simple selection rules apply: $\Delta n = 0$ and $\Delta L = 0$. The strengths of the transitions are directly proportional to the degeneracies, i.e., $(2L+1)$.

Although reasonably accurate for describing the energy of the fundamental optical transition in materials where $0 < 2\gamma_2/\gamma_1 < 0.7$,²¹ this approach does not properly account for the energies and relative strengths of the variety of excited transitions. In fact, for a better description of small crystallites, one must take into account the confinement-induced valence-band mixings.

We follow and develop the analytical procedure introduced in Ref. 23: The unknown valence-band wave functions are expanded over a set of several Bloch states, multiplied by envelope functions. For rather wide-band-gap materials, the matrix representation of the valence-band Hamiltonian—the so-called Kane matrix—can be restricted to the basis of the only valence-band $|J, m_J\rangle$ Bloch states ($J = \frac{3}{2}$, $m_J = \pm \frac{3}{2}$ and $\pm \frac{1}{2}$, for light and heavy holes, $J = \frac{1}{2}$, $m_J = \pm \frac{1}{2}$, for the SO band). The corresponding 6×6 Hamiltonian matrix is well known: we keep the same notations as in Ref. 23.

B. Two-band approximation

Several authors have assumed no mixing between the upper valence bands and the SO band.^{18,21,24} In this case, one can restrict the valence-band Hamiltonian to the four upper valence states, the so-called light-hole and heavy-hole bands.

As stated above, the Hamiltonian commutes²⁶ with operator $F = J + L$. The Luttinger-Kohn Hamiltonian can be turned from its matrix representation in the $|J, m_J\rangle$ basis into its matrix representation in the basis of eigenstates of F and F_z [to each value of F correspond $(2F+1)$ values for F_z]. This is done by calculating the Clebsch-Gordan coefficients corresponding to the addition of $J = \frac{3}{2}$ and $L = 0, 1, 2, \dots$. The result is a block-diagonal matrix: in each subspace corresponding to $F = \frac{1}{2}, \frac{3}{2}, \frac{5}{2}, \dots$ one gets $(2F+1)$ identical 4×4 matrices, which can be written, in fact, as $(2F+1)$ pairs of 2×2 blocks. Each of these blocks corresponds to the mixing of two basis states such as $|F, F_z, \frac{3}{2}, L\rangle$ and $|F, F_z, \frac{3}{2}, L+2\rangle$.

Instead of pure S -, P -, D -like (etc.) states, one gets couplings between states whose quantum numbers L differ by 2. The most general expression of quantized states in the semiconductor sphere is a combination of orthogonal basis states of the “ F subspace,” multiplied by spherical Bessel functions $j_L(Kr)$ and $j_{L+2}(Kr)$.

For instance, for $L=\frac{3}{2}$ and whatever F_z , using the compact notation $|F, F_z, J, L\rangle = |J, L\rangle$, the diagonalization of one of the two blocks corresponds to the coupling of S ($L=0$) and D ($L=2$) states. One gets the following eigenstates:

$$\begin{aligned} |\Psi_{\text{LH}}\rangle &= \sqrt{\frac{1}{2}}[|\frac{3}{2}, 0\rangle - |\frac{3}{2}, 2\rangle], \\ |\Psi_{\text{HH}}\rangle &= \sqrt{\frac{1}{2}}[|\frac{3}{2}, 0\rangle + |\frac{3}{2}, 2\rangle], \end{aligned} \quad (1)$$

and one thus obtains the following light-hole- and heavy-hole-like “envelope vectors,” written on the basis of the $|\frac{3}{2}, L\rangle$ states:

$$\phi_{\text{LH}}(r) = \sqrt{\frac{1}{2}} \begin{bmatrix} j_0(K_{\text{LH}}r) \\ -j_2(K_{\text{LH}}r) \end{bmatrix}, \quad \phi_{\text{HH}}(r) = \sqrt{\frac{1}{2}} \begin{bmatrix} j_0(K_{\text{HH}}r) \\ j_2(K_{\text{HH}}r) \end{bmatrix}. \quad (2)$$

Whatever F , the wave vectors K_{HH} and K_{LH} are always given by the simple dispersion relations $E = E_v - (\gamma_1 - 2\gamma_2)K_{\text{HH}}^2$ and $E = E_v - (\gamma_1 + 2\gamma_2)K_{\text{LH}}^2$. It is to be noted that the crystal-field splitting of these bands, associated with the hexagonal symmetry of wurtzite semiconductors like CdS or CdSe, is very small compared to the large confinement-induced energy shifts and splittings of the various levels. This splitting will be ignored, in first approximation.

Finally, the most general expression for the valence-band wave function is a normalized linear combination of $\phi_{\text{LH}}(r)$ and $\phi_{\text{HH}}(r)$. The condition of vanishing of this wave function at the surface of the crystallite ($r=R$) provides the quantized levels. Though the change of basis set and the calculation of all matrix elements are a bit tedious, the diagonalization of each block is straightforward and the final result is quite simple. The states in each subspace (up to $F = \frac{7}{2}$), their F_z degeneracies, and the corresponding equations to be solved are summarized below:

$$P_{1/2} \quad (2) \quad j_1(K_{\text{LH}}R) = 0, \quad (3a)$$

$$D_{1/2} \quad (2) \quad j_2(K_{\text{LH}}R) = 0, \quad (3b)$$

$$SD_{3/2} \quad (4) \quad j_0(K_{\text{HH}}R)j_2(K_{\text{LH}}R) + j_0(K_{\text{LH}}R)j_2(K_{\text{HH}}R) = 0, \quad (3c)$$

$$PF_{3/2} \quad (4) \quad 9j_1(K_{\text{HH}}R)j_3(K_{\text{LH}}R) + j_1(K_{\text{LH}}R)j_3(K_{\text{HH}}R) = 0, \quad (3d)$$

$$PF_{5/2} \quad (6) \quad 2j_1(K_{\text{HH}}R)j_3(K_{\text{LH}}R) + 3j_1(K_{\text{LH}}R)j_3(K_{\text{HH}}R) = 0, \quad (3e)$$

$$DG_{5/2} \quad (6) \quad 6j_2(K_{\text{HH}}R)j_4(K_{\text{LH}}R) + j_2(K_{\text{LH}}R)j_4(K_{\text{HH}}R) = 0, \quad (3f)$$

$$DG_{7/2} \quad (8) \quad 5j_2(K_{\text{HH}}R)j_4(K_{\text{LH}}R) + 9j_2(K_{\text{LH}}R)j_4(K_{\text{HH}}R) = 0. \quad (3g)$$

The labeling of the states has been introduced in Sec. I. Each equation has an infinite number of solutions labeled by the principal quantum number n ($n=1,2,\dots$). The ground state is always the $1SD_{3/2}$.^{18,21–24} The energetic ordering of the excited states strongly depends on the values of Luttinger parameters γ_1 and γ_2 , as do the oscillator strengths of the optical transitions from these states to conduction-band quantized levels.

Equations (3a)–(3d) have already been given in Ref. 23. Solving these equations is straightforward, if compared to usual methods using all-numerical expansion-diagonalization procedures. We also remark the presence of state $D_{1/2}$ [Eq. (3b)], which derives from the formalism of Ref. 23. For some reason, this state is not mentioned in several previous works.^{21,24}

The absorption spectrum of a crystallite is constituted by a series of peaks which correspond to the transitions between conduction and valence quantized levels. The allowed interband transitions involve initial and final states which possess common L contributions. The oscillator strengths of these transitions are given by the squared matrix element of the dipole moment between the normalized final and initial states. For instance, the fundamental transition is $1SD_{3/2} \rightarrow 1S_e$,^{10,18} and its oscillator strength is

$$\begin{aligned} |\langle 1SD_{3/2} | \mathbf{p} | 1S_e \rangle|^2 &= 8\pi\Pi^2 \left[A \int_0^R j_0(K_{\text{HH}}\rho)j_0(K_e\rho)\rho^2 d\rho \right. \\ &\quad \left. + B \int_0^R j_0(K_{\text{LH}}\rho)j_0(K_e\rho)\rho^2 d\rho \right]^2, \quad (4) \end{aligned}$$

where j_0 is the spherical Bessel function of order 0 and $K_e = \pi/R$ is the wave number of the confined electron, in the $1S_e$ state. $\Pi^2 = |\langle S | p_\xi | \Xi \rangle|^2$ is the squared matrix element of p_ξ ($\xi=x,y,z$) between the conduction band and state $|\Xi\rangle$ ($\Xi=X,Y,Z$).

Allowed transitions also exist between levels originating from the split-off band and the conduction band. Within the present approximation, the simple $\Delta n=0$ and $\Delta L=0$ rules apply, and the oscillator strengths of $S_e - S_{\text{SO}}$, $P_e - P_{\text{SO}}$, ... transitions are equal to $2(2L+1)\Pi^2$.

The optical density of a crystallite of radius R versus the photon energy E is obtained as the sum of all contributions. In first approximation, the electron-hole Coulomb interaction will just be included as a low-energy shift of the absorption lines by a quantity calculated as the matrix element of the Coulomb potential between conduction and valence eigenstates.²⁷ For a realistic modeling⁵ of absorption spectra, we include a homogeneous broadening of absorption peaks

as a Lorentzian function, with a half width at half maximum Γ . In addition, because the experimental quantized exciton peaks are broadened by an inhomogeneous distribution of sizes, we may also assume a Gaussian size-distribution function $P(R)$ with average radius \bar{R} and variance σ^2 .

C. Three-band approximation

We extend the calculations of Ref. 23 to the mixing of the three upper valence bands. The total angular momentum $F=L+J$ remains a good quantum number. We treat explicitly the cases of $F=\frac{1}{2}$ and $\frac{3}{2}$, and go more rapidly to the result for $F=\frac{5}{2}$. We thus obtain analytically the set of equations yielding the valence-band eigenenergies and eigenstates of spherical crystallites, versus their radius R .

In the degenerate subspaces where $F=\frac{1}{2}$, $F_z=\pm\frac{1}{2}$ the valence-band Hamiltonian may be written²³

$$H_{1/2} = \begin{bmatrix} H_{\text{odd}} & 0 \\ 0 & H_{\text{even}} \end{bmatrix}, \quad (5)$$

where blocks $H_{\{\text{odd,even}\}}$ have the form

$$H_{\{\text{odd,even}\}} = \begin{bmatrix} E_v - (\gamma_1 + 2\gamma_2)K^2/2 & -\sqrt{2}\gamma_2K^2 \\ -\sqrt{2}\gamma_2K^2 & E_v - \Delta - \gamma_1K^2/2 \end{bmatrix}. \quad (6)$$

We use the compact notations $|J,L\rangle$ for basis states and the numbers in curly brackets represent the two possibilities for L . These blocks correspond respectively to states denoted $PP_{1/2}$ and $DS_{1/2}$, which are parents of the $P_{1/2}$ and $D_{1/2}$ states of the $2B$ modeling (from now on, the last capital letter will always correspond to the contribution of the SO band). The first block (states $PP_{1/2}$) yields the following eigenstates:

$$|\Psi_{LS_1}\rangle = \frac{1}{\sqrt{\rho^2 - \chi\rho}} \left[2\gamma_2K^2 \left| \frac{3}{2}, 1 \right\rangle - \frac{1}{\sqrt{2}}(\rho - \chi) \left| \frac{1}{2}, 1 \right\rangle \right], \quad (7a)$$

$$|\Psi_{LS_2}\rangle = \frac{1}{\sqrt{\rho^2 + \chi\rho}} \left[2\gamma_2K^2 \left| \frac{3}{2}, 1 \right\rangle - \frac{1}{\sqrt{2}}(\rho + \chi) \left| \frac{1}{2}, 1 \right\rangle \right], \quad (7b)$$

where $\rho = \frac{1}{2}\sqrt{9\gamma_2^2K^4 - 2\gamma_2K^2\Delta + \Delta^2}$ and $\chi = \Delta - \gamma_2K^2$. The eigenenergies are given by

$$E_{LS_1} = E_v - (\Delta/2) - (\gamma_1 + \gamma_2)(K^2/2) + \rho, \quad (8a)$$

$$E_{LS_2} = E_v - (\Delta/2) - (\gamma_1 + \gamma_2)(K^2/2) - \rho. \quad (8b)$$

For the second block ($DS_{1/2}$) the expressions of eigenvalues and eigenstates are absolutely similar. One just has to replace the basis kets by $(|\frac{3}{2}, \frac{1}{2}, 0\rangle, |\frac{1}{2}, 0\rangle)$.

Then we make the same development as in the case of two coupled bands. For a given energy E , states $|\Psi_{LS_1}\rangle$ and $|\Psi_{LS_2}\rangle$, respectively, correspond to wave numbers K_1 and K_2 , which can be derived analytically from Eqs. (8), yielding two sets of values (ρ_1, χ_1) and (ρ_2, χ_2) . The eigenvectors of the first basis ($PP_{1/2}$) may be written from spherical Bessel functions:

$$\phi_i(r) = \frac{1}{\sqrt{\rho_i^2 \mp \chi_i \rho_i}} \begin{bmatrix} 2\gamma_2K_i^2 j_1(K_i r) \\ -1 \\ \frac{1}{\sqrt{2}}(\rho_i \mp \chi_i) j_1(K_i r) \end{bmatrix} \quad (i=1,2). \quad (9)$$

Upper signs correspond to $i=1$ and lower signs to $i=2$. The most general expression of the corresponding valence-band wave function is thus a linear combination of $\phi_1(r)$ and $\phi_2(r)$. Again the condition that the wave function is zero at the surface of the sphere yields the simple equation to be solved. In the case of $PP_{1/2}$ states, this equation can be written

$$(\beta - \theta)j_1(K_1 R)j_1(K_2 R) = 0, \quad (10)$$

where $\beta = K_1^2(\rho_2 + \chi_2)$ and $\theta = K_2^2(\rho_1 - \chi_1)$. With the same readiness, we can write the corresponding equation for $DS_{1/2}$ states:

$$\beta j_2(K_1 R)j_0(K_2 R) - \theta j_2(K_2 R)j_0(K_1 R) = 0. \quad (11)$$

We shall now present the fourfold degenerate case of $F=\frac{3}{2}$ ($F_z=\pm\frac{1}{2}, \pm\frac{3}{2}$). The corresponding sub-Hamiltonian $H_{3/2}$ can be written in the same form as Eq. (5), where the sub-blocks are given by

$$H_{\text{even}} = \begin{bmatrix} E_v - \gamma_1 K^2/2 & \gamma_2 K^2 & \gamma_2 K^2 \\ \gamma_2 K^2 & E_v - \gamma_1 K^2/2 & -\gamma_2 K^2 \\ \gamma_2 K^2 & -\gamma_2 K^2 & E_v - \Delta - \gamma_1 K^2/2 \end{bmatrix} \quad (12a)$$

and

$$H_{\text{odd}} = \begin{bmatrix} E_v - (\gamma_1/2 - 4\gamma_2/5)K^2/2 & 3\gamma_2K^2/5 & \gamma_2K^2/\sqrt{5} \\ 3\gamma_2K^2/5 & E_v - (\gamma_1/2 + 4\gamma_2/5)K^2/2 & -3\gamma_2K^2/\sqrt{5} \\ \gamma_2K^2/\sqrt{5} & -3\gamma_2K^2/\sqrt{5} & E_v - \Delta - \gamma_1K^2/2 \end{bmatrix}. \quad (12b)$$

The diagonalizations of these matrices yield an uncoupled heavy-hole-like state $|\Psi_{\text{HH}}\rangle$ and two mixed states $|\Psi_{LS_1}\rangle$ and $|\Psi_{LS_2}\rangle$ involving light-hole and split-off-like bands.

Let us detail the case of block H_{even} , corresponding to $SDD_{3/2}$ states. The diagonalization yields the following solutions:

$$|\Psi_{\text{HH}}\rangle = (|\frac{3}{2}, 0\rangle + |\frac{3}{2}, 2\rangle) / \sqrt{2},$$

$$|\Psi_{LS_1}\rangle = \frac{1}{\sqrt{\rho^2 - \chi\rho}} [\gamma_2 K^2 |\Psi_{LS'}\rangle + \frac{1}{\sqrt{2}} (\rho - \chi) |\frac{1}{2}, 2\rangle],$$

$$|\Psi_{LS_2}\rangle = \frac{1}{\sqrt{\rho^2 + \chi\rho}} [\gamma_2 K^2 |\Psi_{LS'}\rangle - \frac{1}{\sqrt{2}} (\rho + \chi) |\frac{1}{2}, 2\rangle], \quad (13)$$

where $|\Psi_{LS'}\rangle = (|\frac{3}{2}, 0\rangle - |\frac{3}{2}, 2\rangle) / \sqrt{2}$.

Concerning the dispersion relations, E_{LS_1} and E_{LS_2} have rigorously the same expressions as above [Eqs. (8)]. For the heavy-hole-like band, one has

$$E_{\text{HH}} = E_v - (\gamma_1 - 2\gamma_2) K^2 / 2. \quad (14)$$

For a given energy E these equations provide three wave numbers K_{HH} , K_1 , and K_2 . The general threefold wave functions, in the basis of the $|J, L\rangle$ states, are

$$\phi_{\text{HH}}(r) = \frac{1}{\sqrt{2}} \begin{bmatrix} j_0(K_{\text{HH}}r) \\ j_2(K_{\text{HH}}r) \\ 0 \end{bmatrix},$$

$$\phi_1(r) = \frac{1}{\sqrt{2\rho_1^2 - 2\chi_1\rho_1}} \begin{bmatrix} 2\gamma_2 K_1^2 j_0(K_1r) \\ -2\gamma_2 K_1^2 j_2(K_1r) \\ (\rho_1 - \chi_1) j_2(K_1r) \end{bmatrix},$$

and

$$\phi_2(r) = \frac{1}{\sqrt{2\rho_2^2 + 2\chi_2\rho_2}} \begin{bmatrix} 2\gamma_2 K_2^2 j_0(K_2r) \\ -2\gamma_2 K_2^2 j_2(K_2r) \\ -(\rho_2 + \chi_2) j_2(K_2r) \end{bmatrix}. \quad (15)$$

The most general expression of the wave function is again a normalized combination of these states, and the boundary condition at $r=R$ provides the equation for $SDD_{3/2}$ levels:

$$j_2(K_{\text{HH}}R) [\beta j_0(K_1R) j_2(K_2R) + \theta j_2(K_1R) j_0(K_2R)] + j_0(K_{\text{HH}}R) j_2(K_1R) j_2(K_2R) (\beta + \theta) = 0. \quad (16)$$

For the second subblock the procedure is identical. The dispersion relations are the same, and the eigenvectors are

$$|\Psi_{\text{HH}}\rangle = (3|\frac{3}{2}, 1\rangle + |\frac{3}{2}, 3\rangle) / \sqrt{10},$$

$$|\Psi_{LS_1}\rangle = \frac{1}{\sqrt{\rho^2 - \chi\rho}} [\gamma_2 K^2 |\Psi_{LS'}\rangle + \frac{1}{\sqrt{2}} (\rho - \chi) |\frac{1}{2}, 1\rangle],$$

$$|\Psi_{LS_2}\rangle = \frac{1}{\sqrt{\rho^2 + \chi\rho}} [\gamma_2 K^2 |\Psi_{LS'}\rangle - \frac{1}{\sqrt{2}} (\rho + \chi) |\frac{1}{2}, 1\rangle], \quad (17)$$

where $|\Psi_{LS'}\rangle = (|\frac{3}{2}, 1\rangle - 3|\frac{3}{2}, 3\rangle) / \sqrt{10}$.

The energies and wave functions of $PF_{3/2}$ states are obtained by solving

$$9j_1(K_{\text{HH}}R) [\beta j_1(K_1R) j_3(K_2R) + \theta j_3(K_1R) j_1(K_2R)] + j_3(K_{\text{HH}}R) j_1(K_1R) j_1(K_2R) (\beta + \theta) = 0. \quad (18)$$

We shall finish with the case of the sixfold $F = \frac{5}{2}$ Hamiltonian, which is again made of two independent 3×3 blocks. Two types of states are produced: $PF_{5/2}$ and $DGD_{5/2}$. The dispersion relations are the same as above. For $PF_{5/2}$ states, we get

$$3j_3(K_{\text{HH}}R) [\beta j_1(K_1R) j_3(K_2R) + \theta j_3(K_1R) j_1(K_2R)] + 2j_1(K_{\text{HH}}R) j_3(K_1R) j_3(K_2R) (\beta + \theta) = 0. \quad (19)$$

For $DGD_{5/2}$ states one has to solve

$$6j_2(K_{\text{HH}}R) [\beta j_4(K_1R) j_2(K_2R) + \theta j_2(K_1R) j_4(K_2R)] + j_4(K_{\text{HH}}R) j_2(K_1R) j_2(K_2R) (\beta + \theta) = 0. \quad (20)$$

Equations (10), (11), (16), and (18)–(20) ($F = \frac{1}{2}, \frac{3}{2}$ and $\frac{5}{2}$) are sufficient to obtain a satisfactory description of the states involved in the absorption spectrum of the crystallite, within ~ 1 – 2 eV above the band-gap energy. The oscillator strengths of the various allowed transitions are calculated exactly as in the preceding section, by using the relevant normalized envelope functions.

III. RESULTS AND DISCUSSION

The numerical parameters used in the following calculations, for the five considered binaries (CdTe, CdSe, CdS, GaAs, and InP), are gathered in Table I.

A. Size dependence of valence-band levels

Similar to the presentations of Refs. 20 and 22, Figs. 1–5 display the calculated energies of valence-band states in spherical nanocrystals, versus $(1/R)^2$. Figure 1 shows the results of both the $2B$ (a) and $3B$ (b) models, in the case of CdTe nanocrystals. Figure 1(a) shows that, although the upper valence-band levels are coupled in the $2B$ modeling, their energies all vary linearly with $(1/R)^2$. Oppositely, the variation of the energy levels is found quite more complex by the $3B$ calculation [Fig. 1(b)]. This is caused by numerous anticrossings between levels of the same symmetry, i.e., levels with common L and F values (see, e.g., in Fig. 1, the crossing between states $1PP_{1/2}$ and $2PFP_{3/2}$). In our notations, as mentioned above, the last capital letter always corresponds to the component related to the SO band. For instance, the $1SDD_{3/2}$ state is affiliated to the well-known $1SD_{3/2}$ state, calculated by the $2B$ modeling,^{14,18,21,24} but with an additional “ D contribution” from the SO band.

In the case of Fig. 1, the large Δ value of CdTe allows one to analyze such anticrossings. The levels which shift rapidly to energies close to Δ exhibit very strong couplings with the SO band. For instance, the $1D_{1/2}$ and $2D_{1/2}$ $2B$ levels acquire a substantial S contribution, even for rather large radii. The resulting $1DS_{1/2}$ and $2DS_{1/2}$ $3B$ levels thus show a broad curvature of their energy shift vs $(1/R)^2$. The other $DS_{1/2}$ states show several small anticrossings, the place of which roughly mark where the $1S_{\text{SO}}$ level of a one-band modeling would have been. However, Fig. 1 demonstrates that the SO band has also a sizable influence on levels lying

TABLE I. Material parameters used in our calculations. E_g is the interband energy gap at liquid-helium temperature (the average for light- and heavy-holes in binaries with usual wurtzite structure). ϵ_r is the relative dielectric constant, used in calculations of the Coulomb interaction. Asterisks mark Luttinger parameters which were deduced from effective-mass values, by using the following expressions: $\gamma_1 = (2/m_{h_\perp} + 1/m_{h_z})/3$, $\gamma_2 = (1/m_{h_\perp} - 1/m_{h_z})/3$, or $\gamma_1 = (1/m_{h_\perp} + 1/m_{l_\perp})/2$; $\gamma_2 = (1/m_{h_\perp} - 1/m_{l_\perp})/2$. In these equations m_h (m_l) correspond to the Γ_9 (Γ_7) bands of the wurtzite structures of CdS or CdSe; z and \perp denote directions parallel and perpendicular to the c axis of these materials.

Material	E_g (eV)	Δ (eV)	ϵ_r	γ_1	γ_2	m_e
CdS	2.590 ^a	0.068 ^a	8.58 ^b	1.09 ^{a,b}	0.34 ^{a,b,*}	0.200 ^a
CdSe	1.853 ^a	0.420 ^a	9.5 ^a	1.67 ^{a,*}	0.56 ^{a,*}	0.120 ^a
CdTe	1.606 ^c	0.927 ^b	9.3 ^c	5.23 ^e	1.89 ^e	0.096 ^c
GaAs	1.519 ^a	0.340 ^a	12.55 ^{a,c}	6.85 ^a	2.10 ^a	0.067 ^a
InP	1.424 ^c	0.108 ^d	12.35 ^c	5.22 ^f	1.83 ^f	0.080 ^c

^aReference 28.

^bReference 29.

^cReference 30.

^dReference 31.

^eReference 32.

^fReference 33.

at much lower energies, namely, the so-called ‘‘odd’’ states ($PF_{3/2}$ and $PP_{3/2}$), as discussed below. This result is related to the large value of the coupling parameter $\gamma = 2\gamma_2/\gamma_1$, in CdTe. Such importance of effective masses has been evoked in Refs. 19 and 22. Indeed, this parameter controls not only the coupling between the two upper valence bands,²¹ but also, to a large extent, the coupling of these bands with the SO bands, since off-diagonal terms in the Hamiltonian are proportional to γ_2 .

Figure 2 illustrates this strong influence of effective-mass parameters on the result of the $3B$ calculation, in the case of CdSe crystallites. The complex system of crossings and anticrossings is found completely different in Figs. 2(a) and 2(b), while the only γ_1 parameter has been changed—in (a) we have taken the value of Table I; in (b) we have used the value proposed in Ref. 34. The currently poor knowledge of CdSe valence-band parameters may have important consequences on the reliability of some theoretical predictions, as shown below. This is essentially due to (i) the fact that Luttinger parameters are only indirectly related to effective masses, and (ii) the attempt which is made to treat CdSe as a material with a zinc-blende structure, while the few available data are all related to wurtzite CdSe. This problem is even more serious in the case of CdS, for which a large dispersion of effective-mass values exists in the literature. Figure 3 presents the results of a $3B$ calculation for nanocrystals of this binary, obtained by using the numerical data of Table I. This plot may be compared to those presented in Fig. 1 of Ref. 22, which display the results of assuming three different sets of light- and heavy-hole masses. In Ref. 22, the Luttinger parameters were extracted from mass values by using the following equations: $\gamma_1 = (1/m_h + 1/m_l)/2$, $\gamma_2 = (1/m_l - 1/m_h)/4$, which is only strictly valid if those masses characterize the motion along the c axis of the material.

Fortunately, for materials with usual cubic structure like CdTe, GaAs, or InP, Luttinger parameters are better known, which warrants the quantitative relevance of theoretical predictions. Figures 4 and 5 are the analogs of Fig. 3, for spherical nanocrystals of GaAs and InP, respectively.

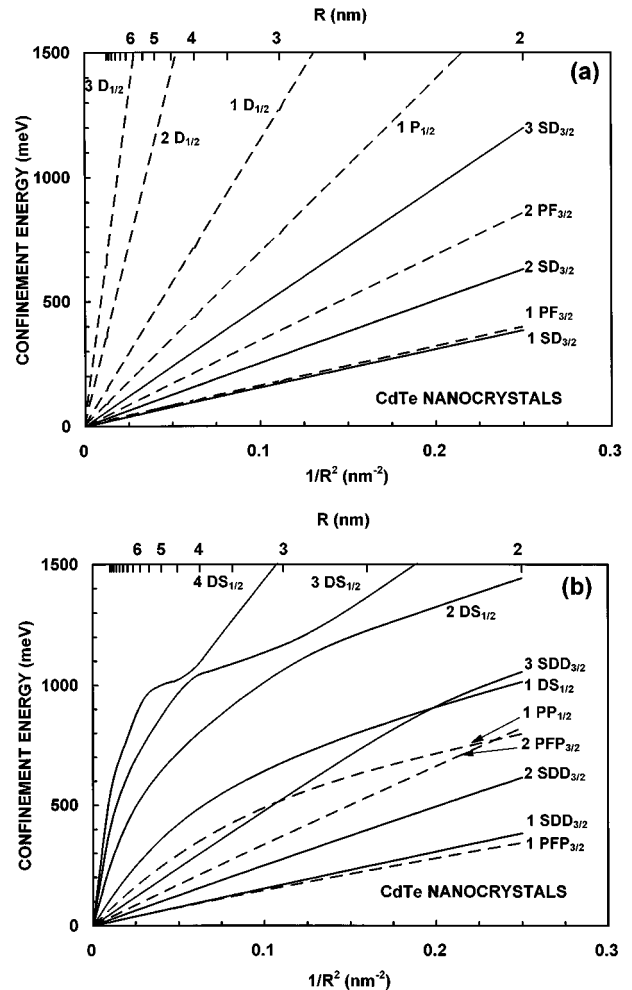


FIG. 1. Plot of the calculated energies of some valence-band levels in spherical CdTe nanocrystals versus $(1/R)^2$, where R is the crystal radius. (a) shows the result of the two-band modeling, while (b) corresponds to the $3B$ approximation. Solid lines (dotted lines) represent levels for which interband transitions are allowed (forbidden) towards the $1S_e$ ground conduction-band level.

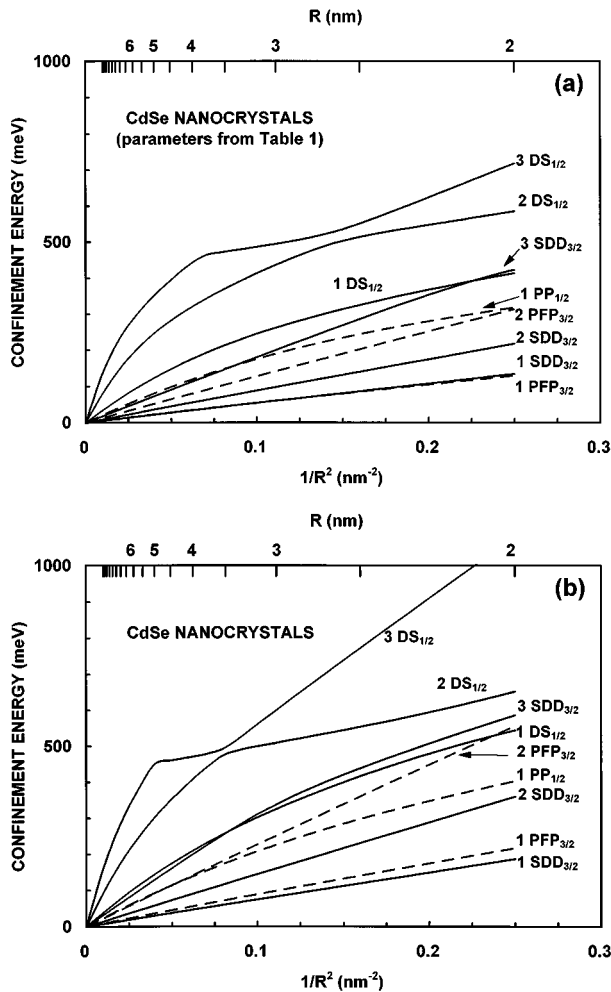


FIG. 2. Energy levels for spherical CdSe nanocrystals versus $(1/R)^2$, calculated within the $3B$ approximation, but by using two sets of material parameters. (a) corresponds to the values of Table I and, in particular, $\gamma_1 = 1.67$. (b) results from the same parameters as for (a) except $\gamma_1 = 2.10$. The assignment of solid and dashed lines is the same as in Fig. 1.

The examination of Figs. 1–5 allows a few general remarks: (i) The influence of the split-off band on energy levels is important, even on the ground levels and even in materials where Δ is large, like CdTe, CdSe, or GaAs. (ii) The results of calculations are extremely sensitive to effective-mass parameters. (iii) When $1/R^2$ is large enough so that most levels overtake the Δ energy, a quasilinear shift of all levels is obtained versus this quantity, because the states lie far enough from their anticrossings. This is particularly true in materials with small spin-orbit splittings, like CdS or InP. On the other hand, for materials with large splittings, like CdTe, complex energy shifts and mixings are present for crystallites of usual sizes.

Coupling effects are even better illustrated by the calculation of the energies and oscillator strengths of the allowed interband optical transitions. As a matter of fact, the oscillator strengths are controlled by the spatial overlap of electron and hole envelope functions, which are more sensitive to mixings than energy levels. Since allowed transitions only occur when a common L character exists between initial and final states, some levels of Figs. 1–5 are represented by solid

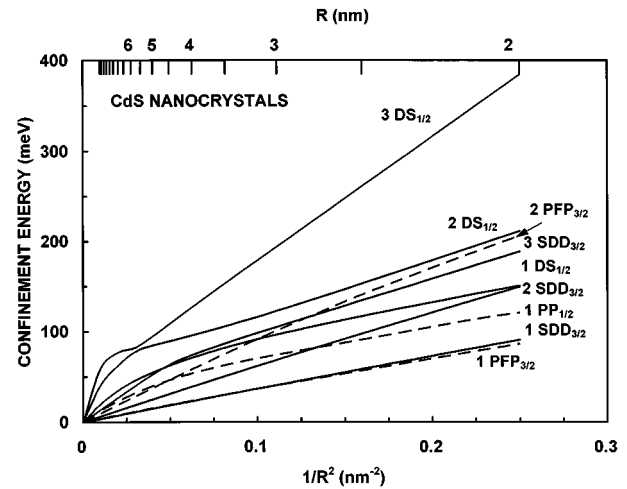


FIG. 3. The analog of Fig. 1(b), for CdS spherical crystallites. This plot is to be compared with those presented in Fig. 1 of Ref. 22. Note that the confinement energies are quite smaller than in crystallites of other binaries, for the same range of radii.

curves: these are levels from which a transition is allowed towards the fundamental $1S_e$ conduction-band state. On the contrary, other valence-band levels give dipole-forbidden transitions with this state: they are shown by dotted curves. Note, in particular, that the S component introduced by the SO band into the $D_{1/2}$ states makes them optically active towards the $1S_e$ state.

B. Absorption spectra

Figure 6 shows the comparison of the two-band and of the three-band modelings in the particular case of CdS crystallites of average radius 2.10 nm, which has been chosen so that the fundamental interband transition is equal to 3.10 eV. In the lower part of the figure, we show the calculated absorption spectrum of a crowd of crystallites having a Dirac distribution as a size-dispersion function, but randomly oriented in space. This corresponds to averaging the spectra over all possible configurations for light polarization against the crystal axes. A Lorentzian broadening parameter $\Gamma = 10$

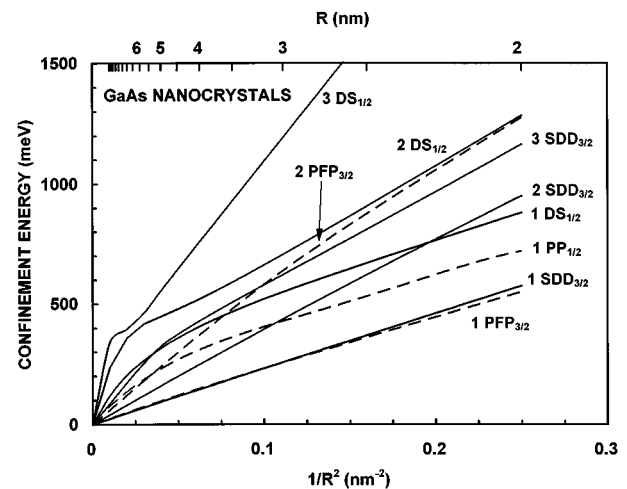


FIG. 4. The same as Fig. 3, for GaAs nanocrystals.

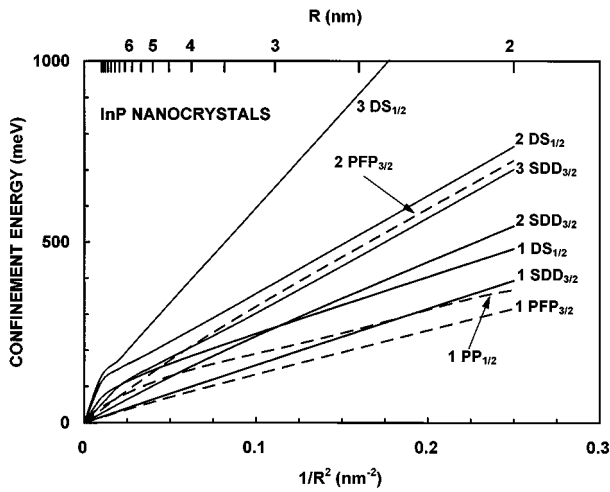


FIG. 5. The same as Fig. 3, for InP nanocrystals.

meV has been assumed. The top of Fig. 6 displays the results obtained for a Gaussian size distribution with the same average radius and with a deviation $\sigma=0.3$ nm, which is compatible with usual experimental findings.

A few transitions have been assigned, for clarity. The peak at low energy is constituted by three transitions, which all involve the $1S_e$ state. Similarly the high-energy peaks are caused by the superimposition of as much as five transitions which involve the $1P_e$ state. Clearly, the present transitions are affiliated to the $1S_e-1S_v$ and $1P_e-1P_v$ transitions which would be calculated by the simple one-band model. Also, there is a sensitive difference between $2B$ and $3B$ approximations, not only in the “single crystallite” spectra, but also in the more realistic broadened spectra. For the present ra-

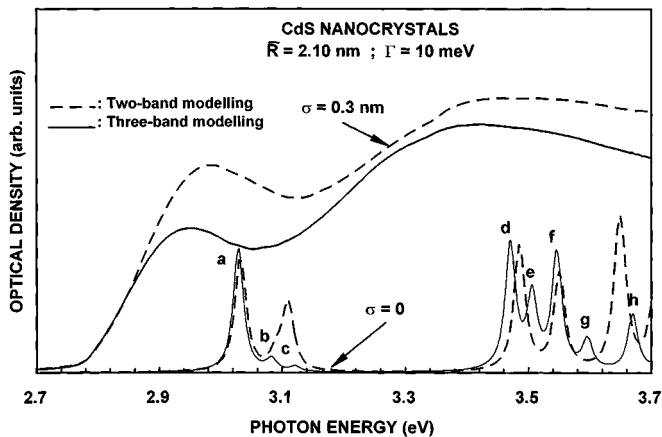


FIG. 6. Calculated absorption spectrum of a crowd of CdS crystallites of average radius 2.10 nm. The interband gap of the system is 3.10 eV. The bottom and the top of the figure correspond to two different size-dispersion functions (bottom: Dirac distribution; top: Gaussian distribution with $\sigma=0.3$ nm). Dashed curves show the results of the two-band approximation, while solid lines correspond to the three-band modeling. Transitions labeled $a-h$ are related to the three-band modeling. They correspond, in this order, to $1S_e-1SDD_{3/2}$, $1S_e-2SDD_{3/2}$, $1S_e-3SDD_{3/2}$, $1P_e-1PFP_{3/2}$, $1P_e-1PP_{1/2}$, $1P_e-1PFF_{5/2}$, $1P_e-2PFF_{5/2}$, $1P_e-3PFF_{5/2}$. For valence-band levels, the last letter corresponds to the L value of the spin-orbit split-off state involved.

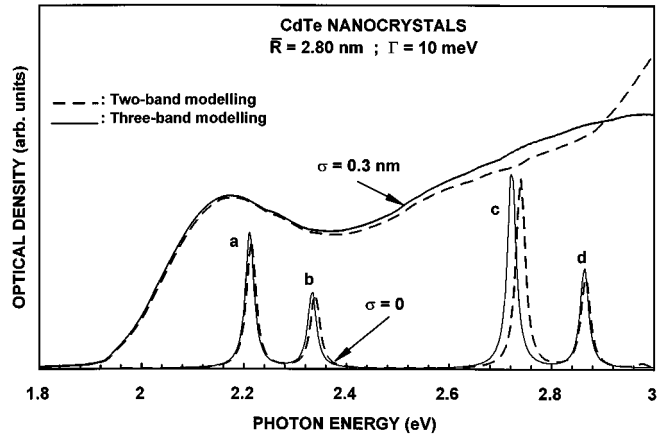


FIG. 7. The same as Fig. 6, for CdTe crystallites of average radius 2.80 nm (interband gap: 2.30 eV). Labels $a-d$ correspond, respectively, to $1S_e-1SDD_{3/2}$, $1S_e-2SDD_{3/2}$, $1P_e-1PFP_{3/2}$, $1P_e-1PFF_{5/2}$, and $1P_e-1PP_{1/2}$.

dus, the energy shift between the two absorption onsets is rather small (~ 30 meV). So, at this stage, it may seem reasonable to state that the complexity of the $3B$ modeling is not necessary if one intends to use it as a fitting procedure, in order to estimate the average crystal radius from an experimental spectrum, for instance.

Let us now compare Figs. 6 and 7 (the latter is analogous to Fig. 6, for CdTe crystallites). The parameters which significantly influence the fine structure of absorption spectra are the Luttinger parameters (γ_1 and γ_2) and the spin-orbit split-off energy Δ . This is the reason why the general aspect of the spectra (see, e.g., the relative positions and intensities of peaks a and b) depend so much on the material. Then, it is very difficult to extract general trends by comparing different materials, since too many things vary from one case to another.

Figure 7 shows that, contrary to what could be expected from Fig. 1, the difference between $2B$ and $3B$ approximations is not large, near the absorption onset. Now, coming to the description of resolved excited states, which can be observed in samples of good quality,¹⁰ the $3B$ modeling is obviously much more accurate. In particular, it is quite clear that the spectral range usually investigated ($\sim 1-2$ eV above the band gap) is by far larger than Δ . Consequently, the spin-orbit split-off band cannot be ignored.

In the $2B$ modeling, the only parameters are γ_1 and γ_2 . The ratio $\gamma=2\gamma_2/\gamma_1$ determines the mixing of valence states,²¹ and thus the relative intensities of the peaks, independently of the crystal size (though the positions of these peaks depend on the crystal radius and on the values of γ_1 and γ_2). In the $3B$ model, the strength of the light-hole-to-split-off-hole coupling is obviously controlled by the value of Δ . However, as noticed above, the γ_2 parameter is also very important: the larger γ_2 the stronger the coupling and thus the larger the difference between the results of the $2B$ and $3B$ approximations. Anyway, concerning *allowed* interband transitions, significant differences only occur at energies of the order of Δ above the absorption onset.

Now, let us investigate different situations. Figures 8–12 show examples of “single-crystallite” spectra calculated for spherical quantum dots of several semiconductors, within the

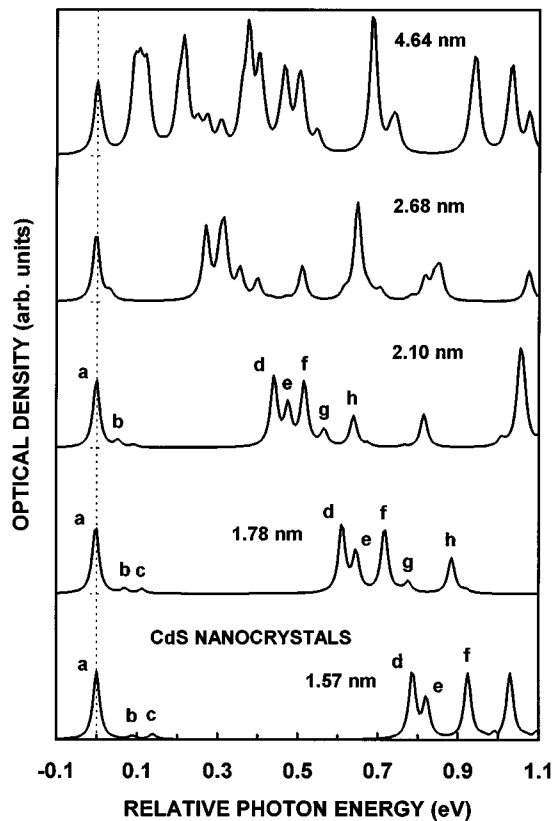


FIG. 8. “Single crystallite” interband absorption spectra of CdS nanocrystals, calculated within the three-band approximation. The radius is indicated near each spectrum. Labels *a–h* correspond to $1S_e-1SDD_{3/2}$, $1S_e-2SDD_{3/2}$, $1S_e-3SDD_{3/2}$, $1P_e-1PP_{3/2}$, $1P_e-1PP_{1/2}$, $1P_e-1PFF_{5/2}$, $1P_e-2PFF_{5/2}$, $1P_e-3PFF_{5/2}$. The fundamental transition energies have been set to zero, for convenience. From the top to the bottom of the figure, these energies are 2.70, 2.90, 3.10, 3.30, and 3.50 eV. The corresponding excitonic energies, obtained within the approximation of Ref. 27, are 2.67, 2.84, 3.03, 3.22, and 3.40, respectively.

3B modeling. The radii indicated near each spectrum have been chosen so that the fundamental interband transition energy varies by regular steps of 0.2 eV. The values for this energy and for the corresponding excitonic energy are indicated in the captions of the figures, since the fundamental interband gap has been set to zero in all cases.

The first remark is that the spectra are extremely size- and material-dependent. Generally speaking, for rather small crystals, the spectra are made of two groups of transitions. These are respectively related to the above-mentioned $1S_e$ and $1P_e$ conduction-band levels. In all cases, the group of excited transitions affiliated to the $1P_e$ state shows a high-energy shift, when decreasing the radius, which is linear with the energy shift of the $1S_e$ -related transitions. Roughly speaking, the excited group shifts approximately twice as fast as the fundamental one. In fact, Figs. 8–12 allow us to observe the competition between two effects. The effect of the only confinement (the “*L* effect”) is responsible for the above rough tendencies, i.e., the shift of groups of lines. In addition, the material manifests itself by adding a fine structure to these global shifts, via what we shall call the “*J* effect.” The latter obviously depends on the Luttinger pa-

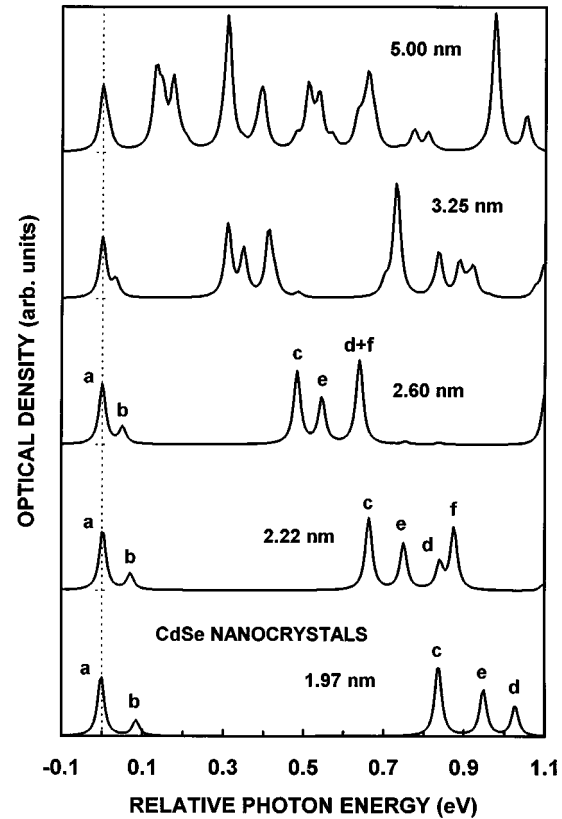


FIG. 9. The same as Fig. 8, for CdSe crystallites. Interband gaps: 2.00–2.80 eV by steps of 0.2 eV. Excitonic gaps: 1.95, 2.12, 2.30, 2.48, and 2.67 eV, respectively. Labels *a–f* correspond, respectively, to $1S_e-1SDD_{3/2}$, $1S_e-2SDD_{3/2}$, $1P_e-1PP_{3/2}$, $1P_e-1PP_{1/2}$, $1P_e-1PFF_{5/2}$, $1P_e-2PFF_{5/2}$.

rameters and on the value of Δ . Here again, it is almost impossible to draw a general trend versus material parameters. Anyway, we can make an interesting comparison between CdTe and InP crystallites. As a matter of fact, both materials happen to have comparable Luttinger parameters, while their Δ values are completely different. It appears that the *L* effect can be clearly observed on InP crystallites because the position of the $1P_e$ group above the fundamental transition is much higher than Δ (~ 0.1 eV), in the present range of radii. On the contrary, for CdTe, $\Delta=0.927$ eV and a much more intricate situation is obtained, for a comparable range of blueshifts of the gap, than for InP. For the same range of small crystallites, in the case of CdS, CdSe, GaAs, or InP, the confinement-induced blueshifts are such that the energy difference between the groups of $1P_e$ and $1S_e$ lines is larger than Δ . Then all confined states lie quite far from their anticrossings and the spectra are rather simple. This is connected to the remark in the preceding section and is confirmed by the direct comparison of Figs. 1(b) and 5: one may state that, by changing energy and radius scales, Fig. 1(b) is a kind of “zoom” into the lower left corner of Fig. 5. In other words, for crystallites of materials with small SO splittings, the *L* effect is dominant and the fine structures of the groups of peaks tend to disappear when reducing the size.

In such cases, increasing the confinement permits one to open wide gaps of transparency between the $1S_e$ and $1P_e$ allowed transitions. When broadened by size-dispersion ef-

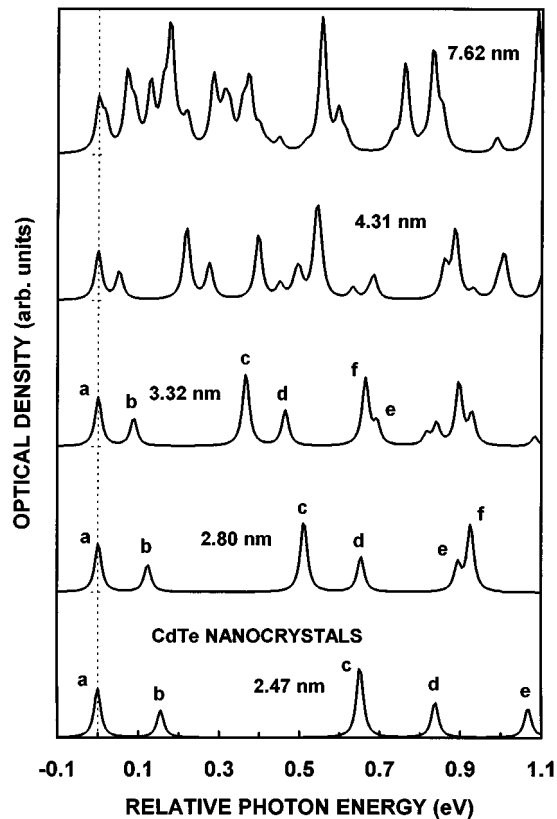


FIG. 10. The same as Fig. 8, for CdTe crystallites. Interband gaps: 1.70–2.50 eV by steps of 0.2 eV. Excitonic gaps: 1.67, 1.84, 2.02, 2.21, and 2.39 eV. The transitions are labeled as in Fig. 7. Labels *e* and *f* correspond, respectively, to $1P_e-1PP_{1/2}$ and $1P_e-2PPF_{5/2}$.

fects, the corresponding absorption spectra are made of two well-separated, poorly structured peaks. This has an interesting consequence, from the experimental viewpoint. As a matter of fact, it may be useful to perform photoluminescence experiments by resonant excitation of size-distributed nanocrystals. This is meant to obtain a selection of the size of the particles. What we see here is that these experiments are likely to be successful in materials such as CdS or InP, where the $1P_e$ resonances are always gathered close to each other and show a very strong sensitivity to the radius. Exciting with a laser tuned at a defined energy above the absorption onset will certainly provide a good selection of the size. For example, for InP crystallites with radii smaller than 5 nm, the $1P_e$ lines are always contained within ~ 0.2 eV. Now, these lines shift with the radius at a rate of ~ 0.8 eV/nm. We thus obtain a theoretical selectivity on the radius smaller than 0.15 nm. For CdS crystallites with R smaller than 2.5 nm, we can estimate from Fig. 8 a selectivity of ~ 0.1 nm.

On the other hand, for CdTe crystallites, even for small radii, many light-hole and heavy-hole states are still in the middle of their crossing with those originating from the split-off band (see Figs. 1 and 10). Then the above groups of lines overlap each other and are less easy to define, even with a size dispersion. In such materials it should be almost impossible to perform a size-selective excitation of the luminescence, because the absorption spectra are made of numerous, well-spanned transitions, which occupy the whole energy

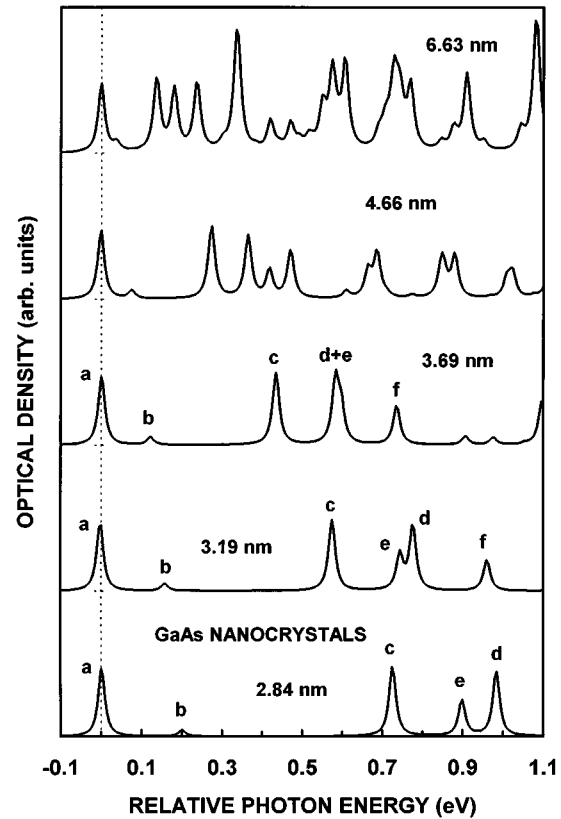


FIG. 11. The same as Fig. 8, for GaAs crystallites. Interband gaps: 1.7–2.5 eV by steps of 0.2 eV. Excitonic gaps: 1.67, 1.86, 2.05, 2.24, and 2.43 eV. Labels *a–f* correspond, respectively, to $1S_e-1SDD_{3/2}$, $1S_e-2SDD_{3/2}$, $1P_e-1PPF_{3/2}$, $1P_e-1PPF_{5/2}$, $1P_e-1PP_{1/2}$, $1P_e-2PPF_{5/2}$.

range of ~ 1.5 eV above the fundamental gap. A laser light is thus likely to be absorbed by crystallites of several sizes.

For “intermediate” cases like CdSe or GaAs, Figs. 8 and 11 show that rather large gaps exist between the two principal series of lines, but the $1P_e$ lines are better resolved and occupy a larger energy range. Fairly good size selectivities can be roughly estimated, especially for radii smaller than ~ 3 nm (~ 4 nm) for CdSe (GaAs), but these values are comparable to the usual values of σ . Selective excitation might be difficult in these cases.

Another remarkable result of $3B$ calculations should not affect absorption experiments, but is rather related with photoluminescence properties, since it rules the allowed or forbidden character of the fundamental interband transition.

C. Allowed or forbidden fundamental transition

Figure 1(b) clearly shows that the ground valence-band level in CdTe crystallites is $1PPF_{3/2}$, whatever the radius (this level is optically inactive with the fundamental $1S_e$ level). This is in complete contradiction with the prediction of the $2B$ modeling by which the ground state is found as the $1SD_{3/2}$, whatever the material and whatever the size.²¹ We thus find that (i) the interband transition of lowest energy, which photoluminescence experiments should reveal, is always symmetry-forbidden in spherical CdTe nanocrystals; (ii) this transition lies at a size-dependent energy—of the order of several tens of meV—below the threshold of the

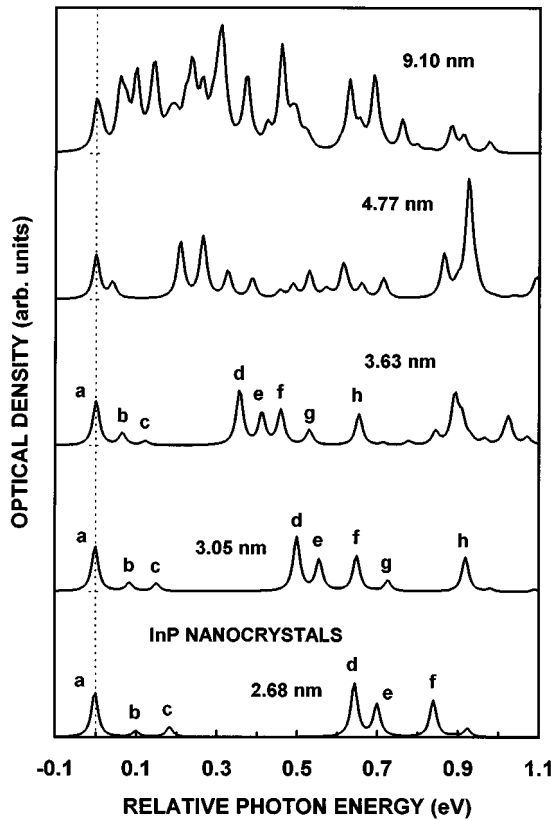


FIG. 12. The same as Fig. 8, for InP crystallites. Interband gaps: 1.5–2.3 eV by steps of 0.2 eV. Excitonic gaps: 1.48, 1.66, 1.87, 2.03, and 2.22 eV. Labels $e-h$ correspond, respectively, to $1S_e-1SDD_{3/2}$, $1S_e-2SDD_{3/2}$, $1S_e-3SDD_{3/2}$, $1P_e-1PFP_{3/2}$, $1P_e-1PP_{1/2}$, $1P_e-1PFF_{5/2}$, $1P_e-2PFF_{5/2}$, $1P_e-3PFF_{5/2}$.

absorption spectrum, i.e., the allowed $1SDD_{3/2}-1S_e$ transition; (iii) the presence of this transition can only be explained by the influence of the spin-orbit split-off band, although the latter lies ~ 1 eV away from the level of interest. Practically, intrinsic luminescence should be hardly observed in CdTe nanocrystals of small size, due to the thermalization of holes onto the $1PFP_{3/2}$ level. The same conclusion can be safely drawn for InP crystallites, as shown by Fig. 5, which suggests that the values of Luttinger parameters are a decisive factor for the symmetry of the ground hole level.

Thus, for crystallites made of the two latter cubic binaries, one expects a luminescence behavior similar to what is usually observed on CdS crystallites,³⁵ for example. As a matter of fact, Grigoryan *et al.*²² have tentatively explained the weak intrinsic luminescence of CdS crystallites by the presence of a comparable forbidden transition. In fact, the case of CdS is often considered specific^{22,25} since $\Delta=68$ meV:²⁸ the strong influence of the split-off band is obvious, while it is neglected for other materials. According to the parameters of Table I, we find that the fundamental transition in CdS crystallites should be the forbidden $1PFP_{3/2}-1S_e$ transition, only for radii smaller than ~ 3 nm, i.e., one excitonic Bohr radius of bulk CdS (see Fig. 3). However, we also find that the allowed $1SDD_{3/2}-1S_e$ transition lies only a few meV above the forbidden one, which is not as demonstrative as in the cases of CdTe and InP, considering the above-mentioned lack of knowledge of Luttinger parameters in CdS. For instance,

Grigoryan *et al.*²² have found the $1PFP_{3/2}-1S_e$ transition fundamental, for two of their three sets of trial parameters. The same remark is valid for CdSe. In Fig. 2, we observe that the ground valence-band state is always the $1SDD_{3/2}$, if one assumes the effective masses of Ref. 34, but the $1PFP_{3/2}$ and $1SDD_{3/2}$ are found almost degenerate if one agrees with the values of Table I.

At the present stage, after several attempts, by using sets of parameters from various authors, we estimate that the situations presented in Figs. 2(a) and 3 are qualitatively relevant. Consequently, the numerical results of the $3B$ modeling seem reasonably coherent with both facts that luminescence in small CdS nanocrystals is usually related to deep trapping of carriers, while it is most probably related to shallow trapping of excitons in small CdSe quantum dots.³⁶ Besides, the presence of an “odd” state as the ground valence-band level had been calculated by Efros and Rodina²⁰ in the asymptotic case where $\Delta=0$. These authors had thus connected the weak luminescence of CdS crystallites to the small value of the spin-orbit splitting. We have shown that this criterion is too restrictive. In a more recent work,²⁵ the same authors have demonstrated that a slight nonsphericity of crystallites yields a size-dependent splitting of the fourfold $1SD_{3/2}$ ground valence-band state, which they considered within the $2B$ approximation (the noncubicity of CdS or CdSe should have the same effect). In some conditions, this was shown to possibly alter luminescence properties of the system. However, from the present study, it seems necessary to (i) try and obtain reliable effective-mass parameters for these materials; and (ii) reconsider the effects of the nonsphericity of crystallites (or the noncubicity of the structure) within the framework of the $3B$ modeling, so as to get reliable quantitative information. Work is at hand on this problem, as well as on the effect of the electron-hole Coulomb interaction on the above results. Actually, Koch *et al.*²⁴ have proved, within a $2B$ approximation, that this interaction may slightly alter valence-band mixings, but they have shown that this should be effective for the larger radii. It is thus most likely that the main features derived here from the $3B$ modeling should be preserved after inclusion of excitonic effects, at least for the smallest nanocrystals.

To be comprehensive, let us finally notice that, for GaAs crystallites, the present $3B$ calculation (see Fig. 4), predicts a critical radius of ~ 3 nm below which $1PFP_{3/2}$ lies at lower energy than the $1SDD_{3/2}$. Experimental evidence of such a critical radius is still desired.

IV. SUMMARY

We have given a set of analytical equations which can be easily solved for calculating the energies and envelope functions of valence-band levels in spherical semiconductor nanocrystals. The Coulomb interaction can be included quite easily as a first-order perturbation, from the envelope functions of electrons and holes. We have applied our modeling to five III–V and II–VI binaries which correspond to practical cases. For all these materials, we have found that including couplings with split-off bands is recommended. When one is only concerned by the determination of the average crystal size from an experimental absorption spectrum, this is restricted to materials with small Δ values. Anyway, this is

crucial for a correct description of transitions between excited states. The analysis of those excited states has allowed us to identify the conditions necessary for an efficient size-selective excitation of the photoluminescence: a rather small Δ value is needed.

We also come to the conclusion that it is too restrictive to focus on the only value of Δ , for including or neglecting spin-orbit split-off states in the calculation of valence-band mixings. In fact, these mixings also strongly depend on Luttinger parameters, which are very different for different ma-

terials. The result is that the split-off band may have a substantial influence on the near-band-gap optical response of spherical semiconductor crystallites, *even in some materials with large spin-orbit splitting energies*, like CdTe. In particular, the relative positions of the most fundamental valence-band levels, and thus intrinsic luminescence, are dependent on the coupling with the SO band. To this extent, for CdTe crystallites, a forbidden fundamental transition is predicted by the present work, in total contradiction with what the usual two-band calculations predict.

- ¹N. Nogami and A. Nakamura, *Phys. Chem. Glasses* **34**, 109 (1993).
- ²U. Woggon, S. V. Bogdanov, O. Wind, K. H. Schlaad, H. Pier, C. Klingshirn, P. Chatziagorastou, and H. P. Fritz, *J. Cryst. Growth* **138**, 976 (1994).
- ³G. Li and M. Nogami, *J. Appl. Phys.* **75**, 4276 (1994).
- ⁴J. Allègre, G. Arnaud, H. Mathieu, P. Lefebvre, W. Granier, and L. Boudes, *J. Cryst. Growth* **138**, 998 (1994).
- ⁵H. Mathieu, T. Richard, J. Allègre, P. Lefebvre, and G. Arnaud, *J. Appl. Phys.* **77**, 287 (1995).
- ⁶M. C. Klein, F. Hache, D. Ricard, and C. Flytzanis, *Phys. Rev. B* **42**, 11 123 (1990).
- ⁷T. Tokizaki, H. Akiyama, M. Takaya, and A. Nakamura, *J. Cryst. Growth* **117**, 603 (1992).
- ⁸M. G. Bawendi, W. L. Wilson, L. Rothberg, P. J. Carroll, T. M. Jedju, M. L. Steigerwald, and L. E. Brus, *Phys. Rev. Lett.* **65**, 1623 (1990).
- ⁹J. Warnock and D. D. Awschalom, *Phys. Rev. B* **32**, 5529 (1985).
- ¹⁰D. J. Norris, A. Sacra, C. B. Murray, and M. G. Bawendi, *Phys. Rev. Lett.* **72**, 2612 (1994).
- ¹¹V. Esch, K. Kang, B. Fluegel, Y. Z. Hu, G. Khitrova, H. M. Gibbs, S. W. Koch, N. Peyghambarian, L. C. Liu, and S. H. Risbud, *Int. J. Non. Opt. Phys.* **1**, 25 (1992).
- ¹²T. Rajh, O. I. Míćić, and A. J. Nozik, *J. Phys. Chem.* **97**, 11 999 (1993).
- ¹³B. G. Potter, T. H. Simmons, P. Kumar, and G. J. Stanton, *J. Appl. Phys.* **75**, 8039 (1994).
- ¹⁴P. Lefebvre, T. Richard, J. Allègre, H. Mathieu, A. Pradel, J. L. Marc, L. Boudes, W. Granier, and M. Ribes, *Superlattices Microstruc.* **15**, 447 (1994).
- ¹⁵O. V. Salata, P. J. Dobson, P. J. Hull, and J. L. Hutchison, *Appl. Phys. Lett.* **65**, 189 (1994).
- ¹⁶O. I. Míćić, C. J. Curtis, K. M. Jones, J. R. Sprague, and A. J. Nozik, *J. Phys. Chem.* **98**, 4966 (1994).
- ¹⁷Y. Kayanuma, *Phys. Rev. B* **38**, 9797 (1988).
- ¹⁸L. M. Ramaniah and S. V. Nair, *Phys. Rev. B* **47**, 7132 (1993).
- ¹⁹A. I. Ekimov, A. A. Onuschchenko, A. G. Plyukhin, and A. L. Efros, *Zh. Eksp. Teor. Fiz.* **88**, 1490 (1985) [*Sov. Phys. JETP* **61**, 891 (1985)].
- ²⁰A. L. Efros and A. V. Rodina, *Solid State Commun.* **72**, 645 (1989).
- ²¹J. B. Xia, *Phys. Rev. B* **40**, 8500 (1989).
- ²²G. B. Grigoryan, E. M. Kazaryan, A. L. Efros, and T. V. Yazeva, *Sov. Phys. Solid State* **32**, 1031 (1990).
- ²³P. C. Sercel and K. J. Vahala, *Phys. Rev. B* **42**, 3690 (1990).
- ²⁴S. W. Koch, Y. Z. Hu, B. Fluegel, and N. Peyghambarian, *J. Cryst. Growth* **117**, 592 (1992).
- ²⁵A. L. Efros and A. V. Rodina, *Phys. Rev. B* **47**, 10 005 (1993).
- ²⁶A. Baldereschi and N. O. Lipari, *Phys. Rev. B* **8**, 2697 (1973).
- ²⁷L. E. Brus, *J. Chem. Phys.* **79**, 5566 (1983); **80**, 4403 (1984).
- ²⁸*Semiconductors Physics of Group IV Elements and III-V Compounds*, edited by O. Madelung, M. Schulz, and H. Weiss, Landolt-Börnstein, New Series, Group III, Vol. 17, Pt a (Springer Verlag, Berlin, 1982).
- ²⁹M. Aven and J. Prener, *Physics and Chemistry of II-VI Compounds* (North-Holland, Amsterdam, 1967).
- ³⁰R. G. Ulbrich and C. Weisbuch, in *Festkörperprobleme XVIII—Advances in Solid State Physics*, edited by J. Treusch (Vieweg, Braunschweig, 1978), p. 217.
- ³¹J. Camassel, P. Merle, L. Bayo, and H. Mathieu, *Phys. Rev. B* **22**, 2020 (1980).
- ³²P. Lawaetz, *Phys. Rev. B* **4**, 3460 (1971).
- ³³Y. Chen, B. Gil, H. Mathieu, and J. P. Lascaray, *Phys. Rev. B* **36**, 1510 (1987).
- ³⁴M. C. Schanne-Klein, Ph.D. thesis, Ecole Polytechnique, Paris, 1992.
- ³⁵See, for instance, U. Woggon, S. V. Bogdanov, O. Wind, K.-H. Schlaad, H. Pier, C. Klingshirn, P. Chatziagorastou, and H. P. Fritz, *Phys. Rev. B* **48**, 11 979 (1993).
- ³⁶See, for instance, P. A. M. Rodrigues, G. Tamulaitis, P. Y. Yu, and S. H. Risbud, *Solid State Commun.* **94**, 583 (1995).